Applied Catalysis B: Environmental 127 (2012) 300–306

Contents lists available at SciVerse ScienceDirect

Applied Catalysis B: Environmental

journal homepage: www.elsevier.com/locate/apcatb

Templated non-PGM cathode catalysts derived from iron and poly(ethyleneimine) precursors

Alexey Serov, Michael H. Robson, Kateryna Artyushkova, Plamen Atanassov*

Center for Emerging Energy Technologies, Department of Chemical and Nuclear Engineering, 1 University of New Mexico, University of New Mexico, Albuquerque, NM 87131, USA

ARTICLE INFO

Article history:
Received 14 April 2012
Received in revised form 28 August 2012
Accepted 31 August 2012
Available online 7 September 2012

Keywords:
Non-PGM catalysts
Fuel cell
ORR
Cathode

ABSTRACT

A series of oxygen reduction catalysts derived from pyrolyzed iron-containing compounds and a nitrogen-containing polymeric precursor, poly(ethyleneimine), (Fe–PEI) were prepared using a sacrificial support method (SSM). The synthesis includes high-temperature pyrolysis in inert atmosphere of the precursor that has been deposited onto a highly dispersed silica support, followed by etching (dissolving) the oxide support, thus resulting in a templated, self-supported, highly porous material – the non-PGM electrocatalyst. The influence of experimental parameters on the catalytic activity of the oxygen reduction reaction (ORR) in acid media was studied, such as molecular weight of PEI, temperature of the heat treatment, duration of the heat treatment, and the ratio of metal to nitrogen precursor. This series of materials was analyzed and characterized by scanning electron microscopy (SEM), BET method (BET) and XPS in order to establish structural morphology and chemical moieties, which was then correlated to activity. Rotating ring disk electrode (RRDE) experiments were performed to evaluate catalytic activity, and the ring current data was used to conduct a mechanistic study of the material for the ORR. This work has determined that the most influential parameters on activity are the metal to nitrogen precursor ratio, and temperature of the heat treatment. Accelerated durability RDE tests (cycling between 0.2 and 1.1 V) revealed high stability of synthesized materials in acid media.

1. Introduction

Fuel cell technology is a promising alternative to conventional hydrocarbon technology for a range of applications; from automotive propulsion, to combined heat and power, to portable electric devices. There has been a significant, concerted effort by industrial and academic research centers that have greatly improved fuel cell performance and durability. However, certain challenges must be overcome before the technology can make any meaningful penetration into common use. The core of the fuel cell device, the membrane electrode assembly (MEA) typically implies the use of platinum catalysts at the anode and the cathode, which makes a major contribution to the cost of the system.

There are two distinct strategies that may alleviate the high cost of an MEA stack: use either ultra-low loadings of platinum that maximize the catalytically available surface area of the metal, or completely circumvent the use of the precious metal with other materials that perform comparably.

The later strategy has piqued the interest of research groups around the globe, and the number of organizations investigating non-platinum group metal (non-PGM) catalysts has increased dramatically. It is notable, however, that despite the amount of research pertaining to non-PGM catalysts, there has not been extensive studies of anode catalysts [1], but instead the focus has centered on cathodes [2].

It is convenient to classify non-PGM cathodes into three separate categories: materials based on transition metal chalcogenides (mainly ruthenium selenides) [3–10], heteroatomic polymeric precursors [11–13], and small molecule derived M–N–C frameworks [14–66]. The later of the classes can be further subdivided: one group based on coordinated metal macrocyclic compounds as a sole source for formation of M–N–C networks [13–27], and the second group of materials can be prepared by combining a metal precursor with a nitrogen/carbon precursor or precursors [28–66].

The common synthesis approach for all of the M–N–C classes entails the deposition of precursors (either macrocyclic or mixture of metal–nitrogen–carbon) that have been adsorbed to high surface area carbon blacks, followed by heat treatment under different conditions [2]. It has been shown that heat treatment is a critical step for creating active centers, which become the catalytic sites for the reduction of oxygen [22]. To date, there is no clear understanding about the nature of the active sites, or their role in ORR. The mechanism of oxygen reduction, which can proceed via several pathways, is not well established for this class of catalysts. Despite the fact

* Corresponding author. Tel.: +1 505 277 2640; fax: +1 505 277 5433.
E-mail address: plamen@unm.edu (P. Atanassov).

0926-3373/$ – see front matter © 2012 Elsevier B.V. All rights reserved.
http://dx.doi.org/10.1016/j.apcatb.2012.08.040

that some publications have included calculations of the number of electrons participating in ORR to be close $4e^-$, the authors usually do not specify that the $n \sim 4e^-$ is the overall collected number of electrons, and it be directly related to single site $4e^-$ transfer. Based on our experience with pyrolyzed macrocyclic compounds, oxygen reduction follows a two-stage 2×2 electron mechanism, where first two electrons participate in electroreduction of oxygen to the hydrogen peroxide, followed by further $2e^-$ electroreduction H_2O_2 to water [67].

The present work is devoted to the preparation and characterization of new catalysts based on pyrolyzed Fe–PEI materials. To improve the surface area, porosity, and density of active sites in catalytic material, our group developed the sacrificial support method (SSM) [68,69], and this templating method was employed in this work. In contrast to conventional synthetic approaches, the SSM utilizes sacrificial supports (silica, alumina, etc.), as opposed to carbonaceous materials. After homogeneous dispersion of precursors onto the surface of silica, and the subsequent pyrolysis, the sacrificial support is removed by etching with KOH or HF. The silica etching procedure results in the creation of an inverted morphology to the sacrificial support (creation of well formed porous structures with pore sizes comparable to the diameter of individual particles of silica). Using high surface area amorphous silica allows us to synthesize M–N–C catalysts with high surface areas and densely populated active sites [68,69].

To further improve the activity of the ORR, several crucial experimental parameters were identified and conditions optimized; they are the variation of the molecular weight of PEI, the metal to nitrogen precursor ratio, and the temperature, duration, and temperature ramping rate of the heat treatment. An analysis and characterization was then performed on the synthesized catalyst material by XPS, SEM and BET methods. The reaction kinetics and mechanism of ORR on these materials was analyzed using the RRDE, and the characterized physical features were then correlated to electrochemical performance.

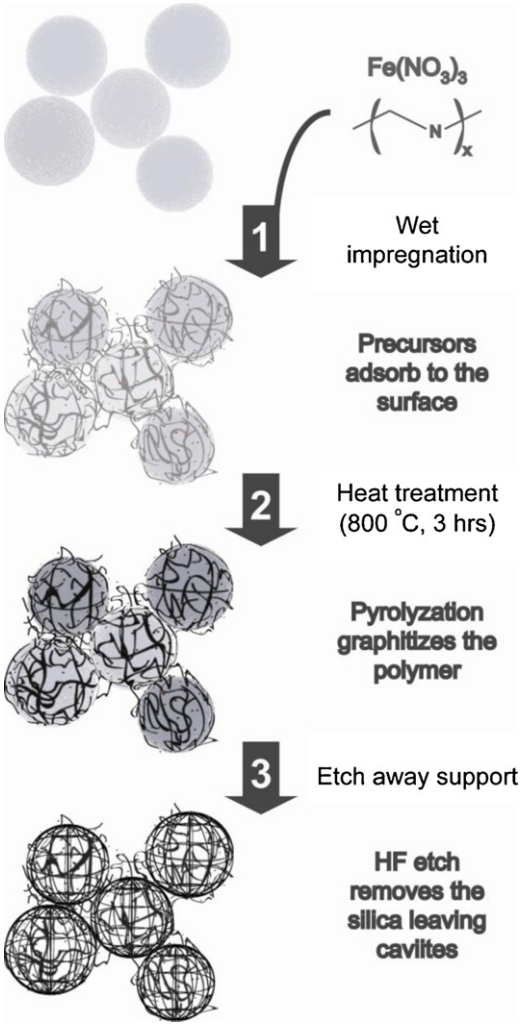

Fig. 1. Schematic representation of the sacrificial support method (SSM).

2. Experimental

2.1. Catalysts preparation

Fe–PEI catalysts were prepared via wet impregnation of iron and poly(ethyleneimine) precursors onto the surface of fumed silica (Cab-O-Sil™ EH-5, surface area: $\sim 400\ m^2\ g^{-1}$). Schematic representation of sacrificial support method is shown in Fig. 1. First, a calculated amount of silica was dispersed in water using the sonobath. Then, a solution of poly(ethyleneimine) (the molecular weights (MW) used were: 2000; 25,000; 600,000; 1,000,000) (Sigma–Aldrich was the source of the PEI and it was used as obtained) in water was added to silica, and sonicated for 20 min. Then, an aqueous solution of iron nitrate ($Fe(NO_3)_3 \cdot 9H_2O$, Sigma–Aldrich) was added to the SiO_2–PEI solution (the total metal loading on silica was calculated to be ~15 wt.%), and then sonicated for 8 h in the sonobath. After sonication, a viscous solution of silica and Fe–PEI was dried overnight at $T = 85\ ^\circ C$. The solid was ground to a fine powder in an agate mortar, and then subjected to the heat treatment (HT). The general conditions of HT were: UHP N_2 atmosphere flowing at a rate of $100\ cc\ min^{-1}$, HT temperatures of 700, 800, and 900 °C, HT temperature ramp rates of 10, 20, and $30\ ^\circ C\ min^{-1}$, and HT durations of 1, 2 and 3 h. Finally, the silica was leached out by means of excess amount of 20 wt.% of HF for 24 h and resulting powder was washed with DI water until neutral reaction. Final metal content after washing with HF was found to be ~0.2–0.3 at.%.

Initially, the iron to PEI ratio selected was 1:2 (by mass), and the catalyst was denoted as Fe–2PEI. In the experiments involving the variation of Fe:PEI ratios, catalysts with Fe–PEI, Fe–2PEI, Fe–3PEI and Fe–4PEI were synthesized (again, the ratios were by mass).

In order to investigate the influence of the SSM on oxygen reduction activity, we synthesized Fe–PEI catalyst by the conventional method whereby it is deposited onto a carbon support (Vulcan XC72R), which has been denoted as sample Fe–2PEI/XC72R. After pyrolysis the prepared material was washed with 20 wt.% of HF.

2.2. Characterization

Scanning electron microscopy was performed on a Hitachi S-800 instrument.

XPS spectra were acquired on a Kratos Axis Ultra X-ray photoelectron spectrometer using a Al Kα source monochromatic operating at 150 W with no charge compensation. The base pressure was about 2×10^{-10} torr, and operating pressure was around 2×10^{-9} torr. Survey and high-resolution spectra were acquired at pass energies of 80 eV and 20 eV, respectively. Acquisition time for survey spectra was 2 min, for C 1s and O 1s spectra – 5 min, for N 1s and Fe 2p – 30 min. Data analysis and quantification were performed using CasaXPS software. A linear background subtraction was used for quantification of C 1s, O 1s and N 1s spectra, while a Shirley background was applied to Fe 2p spectra. Sensitivity factors provided by the manufacturer were utilized. A 70% Gaussian/30% Lorentzian line shape was utilized in the curve-fit of N 1s.

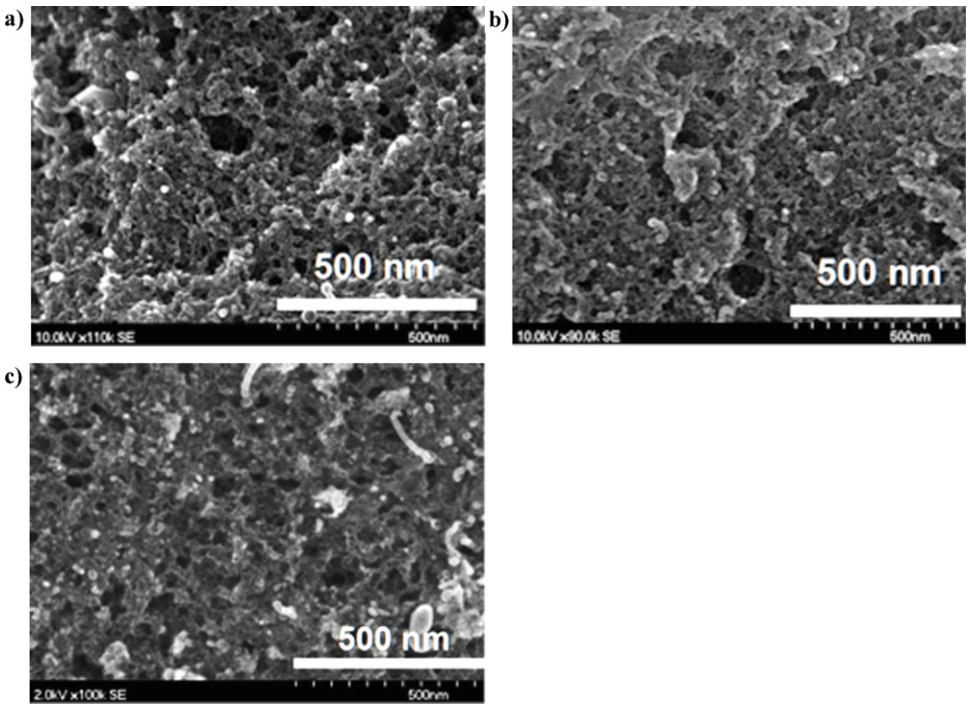

Fig. 2. SEM images for Fe–2PEI (MW = 2000) pyrolyzed at different temperatures. (A) $T = 700\,^{\circ}C$, (B) $T = 800\,^{\circ}C$ and (C) $T = 900\,^{\circ}C$.

2.3. Rotating ring disk electrode (RRDE)

Electrochemical analysis for the synthesized catalysts was performed using the Pine Instrument Company electrochemical analysis system. The rotational speed reported was 1600 RPM, with a scan rate of 20 mV s^{-1}. The electrolyte was 0.5 M H_2SO_4 saturated in O_2 at room temperature. A platinum wire counter electrode and a Ag/AgCl reference electrode were used.

The working electrodes were prepared by mixing 5 mg of the Fe–PEI electrocatalyst with 850 μL of a water and isopropyl alcohol (4:1, volume) mixture, and 150 μL of Nafion® (0.5 wt.%, DuPont). The mixture was sonicated before 20 μL was applied onto a glassy carbon disk with a sectional area of 0.2474 cm^2. The loading of catalyst on the electrode was 0.4 mg cm^{-2}.

2.4. Accelerated durability protocol for non-PGM cathode catalysts

Working electrode was prepared as mentioned above with reduced catalyst loading (0.2 mg cm^{-2}). Electrolyte was 0.1 M H_2SO_4 saturated with O_2. Durability tests were performed at rotation rate of 900 RPM with scan rate 50 mV s^{-1}. Potential range for scanning was selected according the recommendations of the US DOE Fuel Cell Durability Working Group between 0.2 and 1.1 V vs. RHE [70].

3. Results and discussion

Analysis of morphological data for the samples prepared at different temperatures revealed the high porosity of the catalysts, all with similar pore sizes, in the range of 30–70 nm (Fig. 2). This bound range of pore sizes originates from the leaching of individual silica particles, resulting in high surface area. The surface area for all synthesized materials was in excess of 1000 $m^2\,g^{-1}$. Such high surface area can be explained by presence smaller pores, which were formed during decomposition of organic network of PEI. The porous structure and high surface area positively affect the mass transfer of gaseous reagents to the active sites of the catalyst, and allows for the removal of water, which avoids flooding of catalyst.

The dependence of catalytic activity on the HT temperature and PEI molecular weight was investigated by variation of HT at $T = 700$, 800 and 900 °C, and MW of 1,000,000, 600,000, 25,000 and 2000 M_n (Fig. 3(A)–(D)). It was found that, regardless of the molecular weight, that the most active catalysts were synthesized at $T = 800\,^{\circ}C$. The HT temperature is the most crucial parameter for formation of active sites. In general, high temperatures will result in decomposed active sites, while lower temperatures will not be sufficient to form densely populated active moieties. Data for materials with different molecular weights were all pyrolyzed at $T = 800\,^{\circ}C$, and are shown in Fig. 4. It is apparent that the catalytic activity of ORR was not significantly affected by the variation of MW. It also should be mentioned that the material prepared by the conventional method using Vulcan XC72R carbon black as a support is significantly less active in comparison to Fe–PEI made by sacrificial support method, which is indicative of the value of the SSM (Fig. 4).

The influence of the HT ramp rate and the duration of the HT are shown in Figs. 5 and 6. It has been determined that 1 h is sufficient for the formation of the active sites, and a HT ramp rate higher than $10^{\circ}\,min^{-1}$ is needed for preparation of materials that are highly active for oxygen reduction.

Nitrogen content in M–N–C/N–C catalysts also plays important role in the formation of active sites [67,71–73]. However, the role of transition metal in ORR catalysis has yet to be defined. There are two primary assumptions about the participation of the transition metal in active site formation. According to one hypothesis, oxygen reduction active sites are built from C—N moieties, however transition metal can promote formation of these sites [72,73]. The other hypothesis considers the transition metal bound to nitrogen as the intrinsic active center [68,71]. A study of the ratio of Fe–PEI, including samples with no iron added, was performed in order to investigate that effect on catalytic activity (Fig. 7). It can be clearly seen that the iron-free material possesses extremely low activity, whereas addition of iron significantly improves ORR activity. Maximum catalytic activity was found for samples with mass ratio of

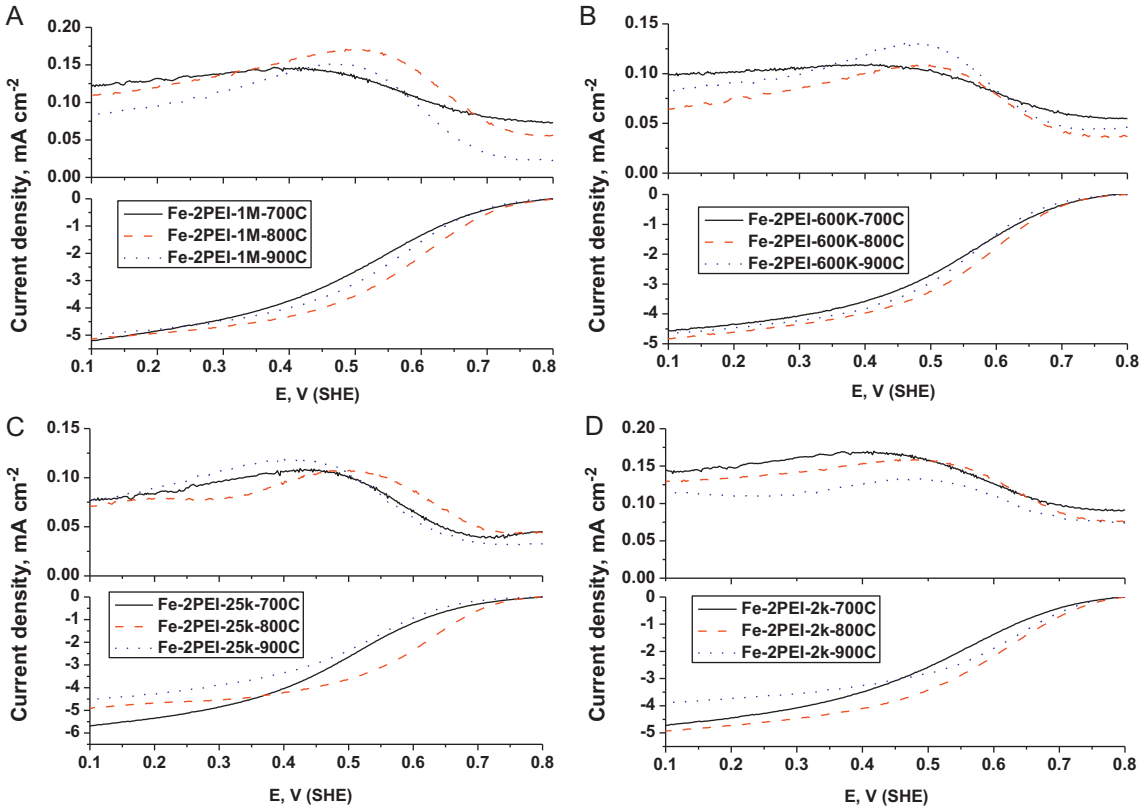

Fig. 3. RRDE data for Fe–2PEI with variation of the molecular weights pyrolyzed at different temperatures: (A) MW = 1,000,000, T = 700 °C (-), T = 800 °C (- - -) and T = 900 °C (···); (B) MW = 600,000, T = 700 °C (-), T = 800 °C (- - -) and T = 900 °C (···); (C) MW = 25,000, T = 700 °C (-), T = 800 °C (- - -) and T = 900 °C (···); and (D) MW = 2000, T = 700 °C (-), T = 800 °C (- - -) and T = 900 °C (···). *Conditions*: 0.5 M H_2SO_4 saturated with O_2, 1600 RPM, 20 mV s^{-1}, catalyst loading 0.4 mg cm^{-2}.

Fe–PEI of 1:3. The carbon materials, which are formed during the thermal decomposition of poly(ethyleneimine), result in a dilution of the active sites when excess PEI is used, leading to decrease of catalytic activity for Fe–4PEI (Fig. 7).

Table 1 and Fig. 8 show results of XPS analysis for the best performing Fe–3PEI sample pyrolyzed at three different temperatures.

As temperature of pyrolysis increases amount of N and O decreases while amount of C increases. For the best performing sample at 800 °C, 5.7 at% of N is detected.

High resolution N 1s spectra has been deconvolved into 6 peaks, main being pyridinic N at 398.8 eV, N coordinated with Fe at 399.9 eV and pyrrolic N at 401 eV. Other types of N typical for these types of materials are cyano group at 398 eV, quaternary and graphitic N at 402.2 and 403.8 eV, respectively [2,53,68]. Even though speciation for all three samples pyrolyzed at three different temperatures is quite similar, the sample at 800 °C has largest amounts of pyridinic N and N associated with Fe, which are the moieties that have been suggested to be one of the possible active sites [68,71,74]. At higher temperature of pyrolysis increase in quaternary, graphitic and pyrrolic N is observed which is accompanied

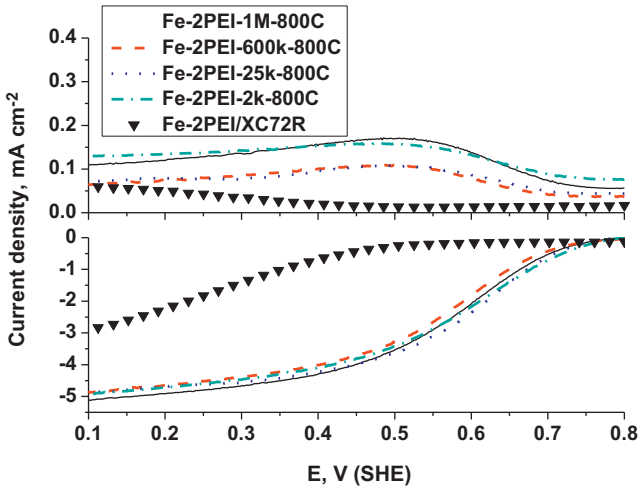

Fig. 4. RRDE data for Fe–2PEI with different MWs heat treated at T = 800 °C compared to Fe–2PEI/XC72R: MW = 1,000,000 (-); MW = 600,000 (- - -); MW = 25,000 (···), MW = 2000 (-·-) and Fe–2PEI/XC72R (▼). *Conditions*: 0.5 M H_2SO_4 saturated with O_2, 1600 RPM, 20 mV s^{-1}, catalyst loading 0.4 mg cm^{-2}.

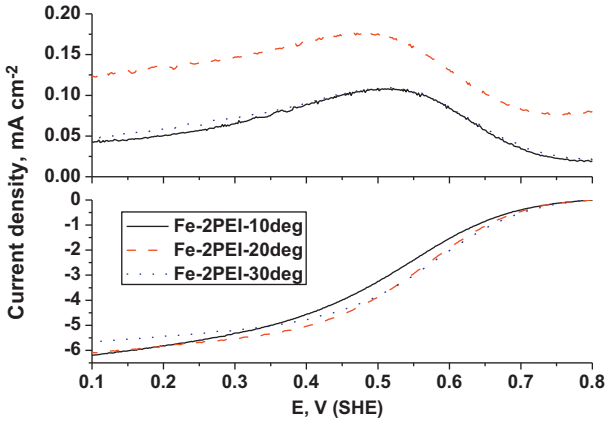

Fig. 5. RRDE data for Fe–2PEI pyrolyzed with different heat treatment ramps (T = 800 °C): Fe–2PEI-10° min^{-1} (-); Fe–2PEI-20° min^{-1} (- - -) and Fe–2PEI-30° min^{-1} (···). *Conditions*: 0.5 M H_2SO_4 saturated with O_2, 1600 RPM, 20 mV s^{-1}, catalyst loading 0.4 mg cm^{-2}.

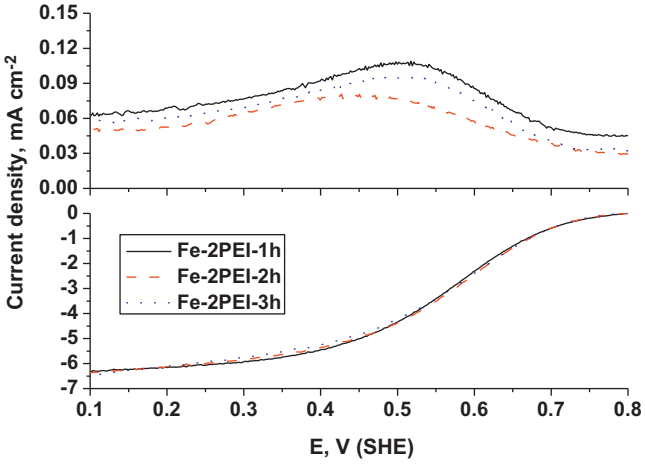

Fig. 6. RRDE data for Fe–2PEI pyrolyzed with different duration of heat treatment: Fe–2PEI-1 h (-); Fe–2PEI-2 h (- - -) and Fe–2PEI-3 h (···). *Conditions*: 0.5 M H_2SO_4 saturated with O_2, 1600 RPM, 20 mV s^{-1}, catalyst loading 0.4 mg cm^{-2}.

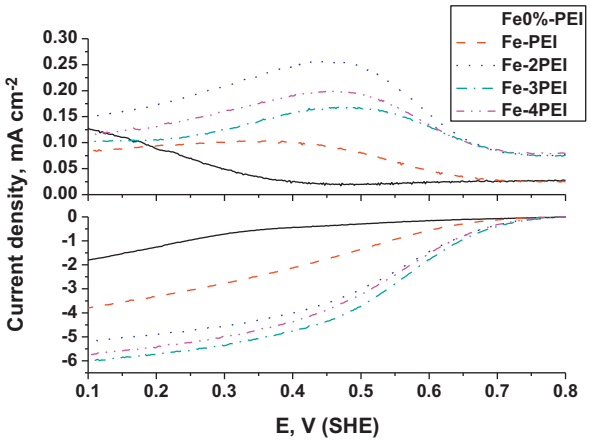

Fig. 7. RRDE data for Fe–PEI synthesized with variation of Fe–PEI ratios: Fe0%–PEI (-); Fe–PEI (- - -); Fe–2PEI (···); Fe–3PEI (-·-) and Fe–4PEI (-···-). *Conditions*: 0.5 M H_2SO_4 saturated with O_2, 1600 RPM, 20 mV s^{-1}, catalyst loading 0.4 mg cm^{-2}.

by the decrease of electrocatalytic activity. It has been shown that pyrrolic and graphitic N are the moieties which promote the $2e^-$ conversion of oxygen to hydrogen peroxide in both metal free and metal-containing electrocatalysts and, therefore compromise the performance of the full $4e^-$ mechanism [75].

RRDE experiments analyzing H_2O_2 production (Eq. (1)) were performed on catalysts with different Fe–PEI ratios (Fig. 9(A)).

$$\%H_2O_2 = 100 * \left(\frac{2 * (I_R/N)}{I_D + I_R/N} \right) \quad (1)$$

where I_R, I_D and N are the ring current, disk current and ring collection efficiency (0.37), respectively.

It was found that the iron-free catalyst yielded more than 50% peroxide (at $V = 0.4$ V), while the H_2O_2 yield for catalysts supplemented with iron was more than twice as low.

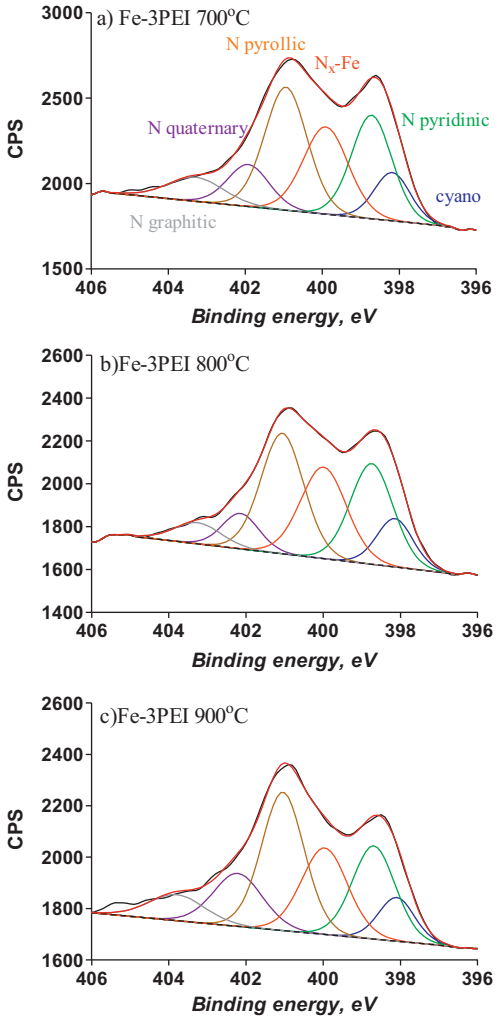

Fig. 8. High resolution N 1s spectra for Fe–3PEI pyrolyzed at (A) 700 °C, (B) 800 °C and (C) 900 °C.

Calculation of the number of electrons transferred per catalytic event was performed using the following equation, and assumes a theoretical maximum of 4 electrons per event:

$$n = \frac{4I_D}{I_D + I_R/N} \quad (2)$$

where n is number of electrons, I_R, I_D and N are the ring current, disk current and ring collection efficiency (0.37), respectively.

Number of electrons calculated by Eq. (2) revealed the fact that the iron-free material reduced oxygen through the mixed $(2 \times 2)e^-$ mechanism (Fig. 9(B)). The addition of iron results in an electron turn-over close to the $4e^-$ (at $V = 0.4$ V). Further studies are needed to establish an oxygen reduction mechanism on Fe–PEI type catalysts.

It is well known that high activity of non-PGM catalysts is critical for being implemented in fuel cells as a suitable substitute for platinum. However, the durability of such catalysts should be

Table 1
Elemental composition and N 1s speciation for three Fe–3PEI samples.

Sample	C 1s %	O 1s %	N 1s %	Fe 2p %	N cyano *398.0*	N pyrid *398.8*	N-Fe *399.9*	N pyrrolic *401*	N qua *402.2*	N graph *403.8*
Fe–3PEI 700 °C	87.5	5.5	6.8	0.2	9.6	23.0	21.6	28.9	9.6	7.4
Fe–3PEI 800 °C	88.5	5.5	5.7	0.2	9.9	24.3	23.8	29.1	7.4	5.6
Fe–3PEI 900 °C	89.9	4.8	5.1	0.2	8.1	20.4	20.4	30.3	13.4	7.4

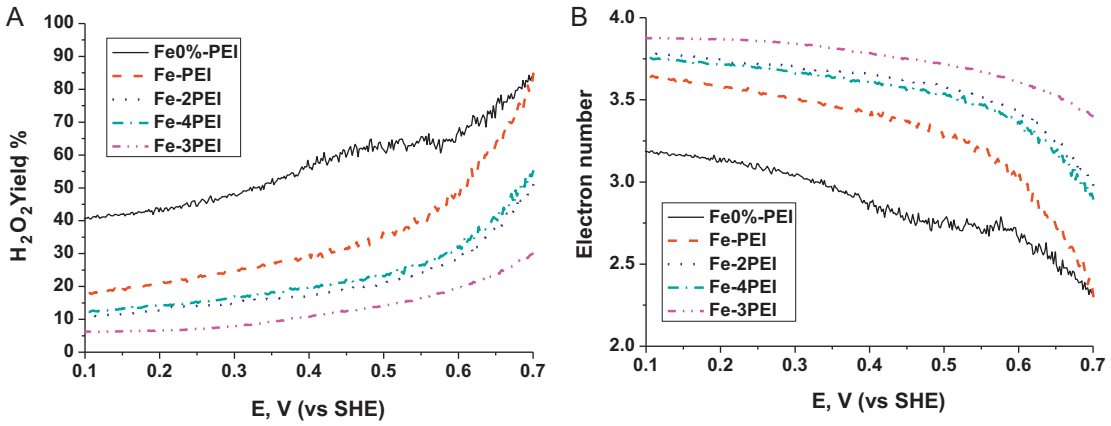

Fig. 9. RRDE data of H_2O_2 production yield and number of electrons in ORR for Fe–PEI synthesized with variation of Fe–PEI ratios: (A) H_2O_2 yield for Fe0%–PEI (-); Fe–PEI (- - -); Fe–2PEI (···); Fe–3PEI (-··-) and Fe–4PEI (-·-) and (B) number of electrons in ORR for Fe0%–PEI (-); Fe–PEI (- - -); Fe–2PEI (···); Fe–3PEI (-··-) and Fe–4PEI (-·-). *Conditions*: 0.5 M H_2SO_4 saturated with O_2, 1600 RPM, 20 mV s^{-1}, catalyst loading 0.05 mg cm^{-2}.

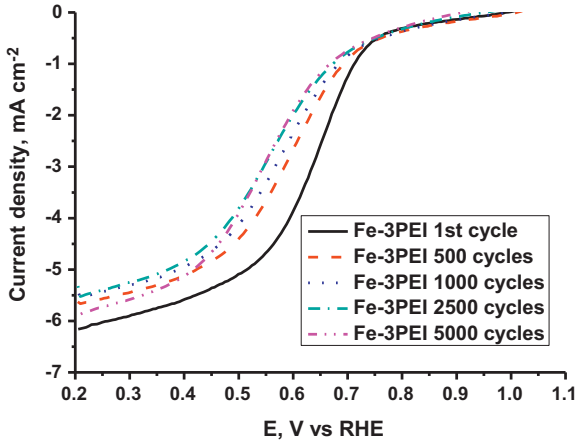

Fig. 10. DoE durability data by RDE method for Fe–3PEI; Fe–3PEI: cycle 1 (—), Fe–3PEI after 500 cycles (- - -), Fe–3PEI after 1000 cycles (···), Fe–3PEI after 2500 cycles (-··-), and Fe–3PEI after 5000 cycles (-···-). *Conditions*: 0.1 M H_2SO_4 saturated with O_2, 900 RPM, 50 mV s^{-1}, catalyst loading 0.2 mg cm^{-2}.

comparable to PGM materials. In order to evaluate the new class of materials based on Fe–PEI, RDE based durability tests were performed under the DoE recommended conditions for non-PGM cathode catalysts [70]. It was determined that the decrease of catalytic activity by measuring $E_{1/2}$ after 5000 cycles was 12.3% (Fig. 10). It also was observed that after 1000 cycles the lost of catalytic activity was negligible and catalyst performed after 1000 cycles as well as after 5000 cycles, what is indicating the exponential loss of activity with increasing number of cycles [76]. Such high durability is very promising for utilization of Fe–AAPyr in a real fuel cell system.

4. Conclusions

Non-PGM catalysts for oxygen reduction were synthesized using the SSM with iron and poly(ethyleneimine) precursors. Full optimization of experimental parameters affecting catalytic activity was performed during this study. It was found that greatest contribution to the final ORR activity arose from HT temperature and the iron to PEI ratio.

It was observed that the morphology of the prepared materials was not affected by HT temperature, and all catalysts exhibited a similarly high surface area and porosity. Surface areas more than 1000 m^2 g^{-1} is derived directly from the SSM, and in combination with highly developed pores structures, it positively affects the density of active sites and promotes beneficial mass transfer properties. Due to the similarity of morphology among all samples generated, the HT parameters (temperature, duration, and ramp rate) affected only the atomic level formation and population of active sites.

Iron-free catalysts possess extremely poor ORR activity, while increasing the ratio of Fe–PEI to the optimal 1:3 greatly improved catalytic activity, but fell off again at higher ratios. It was found in RRDE experiments that full $4e^-$ transfer was not attained for the Fe–PEI class of catalysts, and additional experiments are needed to determination the of nature of active sites. XPS suggests higher relative amounts of pyridinic and N coordinated with Fe for best performing electrocatalysts. Further XAFS/XANES spectroscopic evaluations are currently ongoing.

Prepared materials possess extremely high durability in RDE tests, ending up with about 90% of initial activity (by $E_{1/2}$ value) after 5000 cycles.

Acknowledgement

This work was supported by the DOE-EERE Fuel Cell Technology Program: “Development of Novel Non Pt Group Metal Electrocatalysts for PEM Fuel Cell Applications”.

References

[1] A. Serov, C. Kwak, Applied Catalysis B: Environmental 91 (2009) 1–10.
[2] F. Jaouen, E. Proietti, M. Lefèvre, R. Chenitz, J.-P. Dodelet, G. Wu, H.T. Chung, C.M. Johnston, P. Zelenay, Energy & Environmental Science 4 (2011) 114–130.
[3] A.A. Serov, M. Min, G. Chai, S. Han, S. Kang, C. Kwak, Journal of Power Sources 175 (2008) 175–182.
[4] Y. Feng, A. Gago, L. Timperman, N. Alonso-Vante, Electrochimica Acta 56 (2011) 1009–1022.
[5] D.T. Whipple, R.S. Jayashree, D. Egas, N. Alonso-Vante, P.J.A. Kenis, Electrochimica Acta 54 (2009) 4384–4388.
[6] V. Le Rhun, E. Garnier, S. Pronier, N. Alonso-Vante, Electrochemistry Communications 2 (2000) 475–479.
[7] A.A. Serov, C. Kwak, Catalysis Communications 10 (2009) 1551–1554.
[8] H. Cheng, W. Yuan, K. Scott, D.J. Browning, J.B. Lakeman, Applied Catalysis B: Environmental 75 (2007) 221–228.
[9] A. Ezeta, E.M. Arce, O. Solorza, R.G. González, H. Dorantes, Journal of Alloys and Compounds 483 (2009) 429–431.
[10] K. Suárez-Alcántara, O. Solorza-Feria, Journal of Power Sources 192 (2009) 165–169.
[11] G. Wu, K.L. More, C.M. Johnston, P. Zelenay, Science 322 (2011) 443–447.
[12] B. Rajesh, P. Zelenay, Nature 443 (2006) 63–66.
[13] T.S. Olson, S. Pylyplenko, P. Atanassov, Journal of Physical Chemistry C 114 (2010) 5049–5059.
[14] R. Jasinski, Nature 201 (1964) 1212.
[15] H. Jahnke, M. Schönborn, G. Zimmermann, Topics in Current Chemistry 61 (1976) 133.

[16] V.S. Bagotzky, M.R. Tarasevich, K.A. Radyushkina, O.E. Levina, S.I. Andrusyova, Journal of Power Sources 2 (1977) 233.
[17] S. Gupta, D. Tryk, I. Bae, W. Aldred, E. Yeager, Journal of Applied Electrochemistry 19 (1989) 19.
[18] U.I. Koslowski, I. Abs-Wurmbach, S. Fiechter, P. Bogdanoff, Journal of Physical Chemistry C 112 (2008) 15356.
[19] J. Maruyama, J. Okamura, K. Miyazaki, Y. Uchimoto, I. Abe, Journal of Physical Chemistry C 112 (2008) 2784.
[20] T.S. Olson, K. Chapman, P. Atanassov, Journal of Power Sources 183 (2008) 557.
[21] J.M. Ziegelbauer, T.S. Olson, S. Pylypenko, F. Alamgir, C. Jaye, P. Atanassov, S. Mukerjee, Journal of Physical Chemistry C 112 (2008) 8839.
[22] A.A. Serov, M. Min, G. Chai, S. Han, S.J. Seo, Y. Park, H. Kim, C. Kwak, Journal of Applied Electrochemistry 39 (2009) 1509.
[23] A. Okunola, B. Kowalewska, M. Bron, P.J. Kulesza, W. Schuhmann, Electrochimica Acta 54 (2009) 1954.
[24] U.I. Kramm, I. Abs-Wurmbach, S. Fiechter, I. Herrmann, J. Radnik, P. Bogdanoff, ECS Transactions 25 (2009) 93.
[25] I. Herrmann, U.I. Kramm, S. Fiechter, P. Bogdanoff, Electrochimica Acta 54 (2009) 4275.
[26] I. Herrmann, U.I. Kramm, J. Radnik, S. Fiechter, P. Bogdanoff, Journal of the Electrochemical Society 156 (2009) B1283.
[27] T.S. Olson, B. Blizanac, B. Piela, J.R. Davey, P. Zelenay, P. Atanassov, Fuel Cells 9 (2009) 547.
[28] J.I. Ozaki, S.I. Tanifuji, A. Furuichi, K. Yabutsuka, Electrochimica Acta 55 (2010) 1864.
[29] T.S. Olson, S. Pylypenko, J.E. Fulghum, P. Atanassov, Journal of the Electrochemical Society 157 (2010) B54.
[30] Y. Nabae, S. Moriya, K. Matsubayashi, S.M. Lyth, M. Malon, L. Wu, N.M. Islam, Y. Koshigoe, S. Kuroki, M.A. Kakimoto, S. Myata, J.I. Ozaki, Carbon 48 (2010) 2613.
[31] G. Xu, Z. Li, S. Wang, X. Yu, Journal of Power Sources 195 (2010) 4731.
[32] I. Herrmann, U.I. Kramm, S. Fiechter, V. Brüser, H. Kersten, P. Bogdanoff, Plasma Processes and Polymers 7 (2010) 515.
[33] Y. Tang, B.L. Allen, D.R. Kauffman, A. Star, Journal of the American Chemical Society 131 (2009) 13200.
[34] J.D. Wiggins-Camacho, K.J. Stevenson, Journal of Physical Chemistry C 113 (2009) 19082.
[35] K. Prehn, A. Warburg, T. Schilling, M. Bron, K. Schulte, Composites Science and Technology 69 (2009) 1570.
[36] Z. Chen, D. Higgins, H. Tao, R.S. Hsu, Z. Chen, Journal of Physical Chemistry C 113 (2009) 21008.
[37] J. Maruyama, I. Abe, Journal of the Electrochemical Society 154 (2007) B297.
[38] G. Wu, Z. Chen, K. Artyushkova, F.H. Garzon, P. Zelenay, ECS Transactions 16 (2008) 159.
[39] A. Garsuch, K. MacIntyre, X. Michaud, D.A. Stevens, J.R. Dahn, Journal of the Electrochemical Society 155 (2008) B953.
[40] K. Lee, L. Zhang, H. Lui, R. Hui, Z. Shi, J. Zhang, Electrochimica Acta 54 (2009) 4704.
[41] X. Yuan, X. Zeng, H.J. Zhang, Z.F. Ma, C.Y. Wang, Journal of the American Chemical Society 132 (2010) 1754.
[42] N.P. Subramanian, X. Li, V. Nallathambi, S.P. Kumaraguru, H. Colon-Mercado, G. Wu, J.W. Lee, B.N. Popov, Journal of Power Sources 188 (2009) 38.
[43] V. Nallathambi, J.W. Lee, S.P. Kumaraguru, G. Wu, B.N. Popov, Journal of Power Sources 183 (2008) 34.
[44] G. Liu, X. Li, B.N. Popov, ECS Transactions 25 (2009) 1251.
[45] G. Liu, X. Li, P. Ganesan, B.N. Popov, Electrochimica Acta 55 (2010) 2853.
[46] J.Y. Choi, R.S. Hu, Z. Chen, Journal of Physical Chemistry C 114 (2010) 8048.
[47] X. Li, G. Liu, B.N. Popov, Journal of Power Sources 195 (2010) 6373.
[48] R. Kobayashi, J.I. Ozaki, Chemistry Letters 38 (2009) 396.
[49] J. Maruyama, N. Fukui, M. Kawagushi, I. Abe, Journal of Power Sources 194 (2009) 655.
[50] H.T. Chung, C.M. Johnston, F.H. Garzon, P. Zelenay, ECS Transactions 16 (2008) 385.
[51] H.T. Chung, C.M. Johnston, P. Zelenay, ECS Transactions 25 (2009) 485.
[52] T.E. Wood, Z. Tan, A.K. Schmoeckel, D. O'Neill, R. Atanasoski, Journal of Power Sources 178 (2008) 510.
[53] G. Wu, K. Artyushkova, M. Ferrandon, J. Kropf, D. Meyers, P. Zelenay, ECS Transactions 25 (2009) 1299.
[54] L. Zhang, K. Lee, C.W.B. Bezerra, J. Zhang, J. Zhang, Electrochimica Acta 54 (2009) 6631.
[55] S. Li, L. Zhang, H. Liu, M. Pan, L. Zan, J. Zhang, Electrochimica Acta 55 (2010) 4403.
[56] R. Kothandaraman, V. Nallathambi, K. Artyushkova, S. Calabrese Barton, Applied Catalysis B: Environmental 92 (2009) 209.
[57] J.L. Qiao, L. Xu, L. Ding, R. Baker, X.F. Dai, J.J. Zhang, Applied Catalysis B: Environmental 125 (2012) 197.
[58] H.J. Zhang, X. Yuan, L. Sun, X. Zeng, Q.Z. Jiang, Z. Shao, Z.F. Ma, International Journal of Hydrogen Energy 35 (2010) 2900.
[59] F. Jaouen, S. Marcotte, J.P. Dodelet, G. Lindbergh, Journal of Physical Chemistry B 107 (2003) 1376.
[60] F. Jaouen, M. Lefèvre, J.P. Dodelet, M. Cai, Journal of Physical Chemistry B 110 (2006) 5553.
[61] F. Jaouen, F. Charreteur, J.P. Dodelet, Journal of the Electrochemical Society 153 (2006) A689.
[62] F. Charreteur, F. Jaouen, S. Ruggeri, J.P. Dodelet, Electrochimica Acta 53 (2008) 2925.
[63] M. Lefèvre, J.P. Dodelet, Electrochimica Acta 53 (2008) 8269.
[64] F. Charreteur, F. Jaouen, J.P. Dodelet, Electrochimica Acta 54 (2009) 6622.
[65] M. Lefèvre, E. Proietti, F. Jaouen, J.P. Dodelet, ECS Transactions 25 (2009) 105.
[66] M. Lefèvre, E. Proietti, F. Jaouen, J.P. Dodelet, Science 324 (2009) 71.
[67] T.S. Olson, S. Pylypenko, P. Atanassov, K. Asazawa, K. Yamada, H. Tanaka, Journal of Physical Chemistry C 114 (2010) 5049–5059.
[68] S. Pylypenko, S. Mukherjee, T.S. Olson, P. Atanassov, Electrochimica Acta 53 (2008) 7875–7883.
[69] A. Serov, M.H. Robson, B. Halevi, K. Artyushkova, P. Atanassov, Electrochemistry Communications 22 (2012) 53–56.
[70] http://www1.eere.energy.gov/hydrogenandfuelcells/m/durability_group.html
[71] E. Proietti, F. Jaouen, M. Lefèvre, N. Larouche, J. Tian, J. Herranz, J.-P. Dodelet, Nature Communications 2 (2011), http://dx.doi.org/10.1038/ncomms1427.
[72] K.A. Kurak, A.B. Anderson, Journal of Physical Chemistry C 113 (2009) 6730–6734.
[73] S. Maldonado, K.J. Stevenson, Journal of Physical Chemistry B 109 (2005) 4707–4716.
[74] M. Ferrandon, A.J. Kropf, D.J. Myers, K. Artyushkova, U. Kramm, P. Bogdanoff, G. Wu, C.M. Johnston, P. Zelenay, Journal of Physical Chemistry C 116 (2012) 16001–16013.
[75] K. Artyushkova, B. Halevi, A. Serov, B. Kiefer, P. Atanassov, Abstracts of Papers of the American Chemical Society 243 (2012), 203-FUEL.
[76] Xuguang Li, Gang Liu, B.N. Popov, Journal of Power Sources 195 (2010) 6373–6378.